Application of MoO₃ as an efficient catalyst for wet air oxidation treatment of pharmaceutical wastewater (Experimental and DFT study)

Chen Chen*[1], Ting Cheng[2], Lei Wang[1], Yuan Tian[1], Qin Deng[1], Yisu Shi[1]

[1]School of Environmental and Chemical Engineering, Jiangsu University of Science and Technology, China
[2]School of Environmental Ecology, Jiangsu City Vocational College, China

*Corresponding author's e-mail: chencjust@sina.com

Abstract: In this work, a highly effective catalyst (MoO₃) is synthesized and applied for catalytic wet air oxidation (CWAO) treatment of pharmaceutical wastewater. The catalyst is systematically characterized to investigate the morphology, crystal structure and chemical composition, and the findings demostrated that MoO₃ catalyst is successfully synthesized. The degradation mechanism is also illustrated by the density functional theory (DFT) calculation. The degradation experiments confirm that MoO₃ catalyst exhibits excellent catalytic performance in CWAO, and the removal rate of TOC (Total Organic Carbon) and COD (Chemical Oxygen Demand) is achieved to more than 93%. The catalyst doses, reaction temperature and reaction time have a significant impact on the removal of pollutants. The degradation process of pollutants in CWAO could be satisfactorily fitted by the second-order kinetics. Besides, MoO₃ displays a favorable stability as CWAO catalyst. DFT calculation illustrates that MoO₃ catalyst is a typical indirect band gap semiconductor. Moreover, the high temperature environment provides the thermal excitation energy, which favors to the free electrons nearing Fermi level to escape the material surface, and excites them to the conduction band, then directly reduces the pollutants in CWAO. These findings demonstrate that MoO₃ can be used as an efficient and excellent catalyst for CWAO of pharmaceutical wastewater.

Introduction

In recent years, people pay more attention to the issue of environmental pollution, especially the pollution of organic wastewater. Pharmaceutical wastewater and other industrial wastewater is one of the largest groups of organic wastewater, which is a challenge for researchers to treat properly. Pharmaceutical wastewater is produced in the pharmaceutical process, and it contains high content of a variety of organic pollutants. However, the biodegradability of pharmaceutical wastewater is extremely poor, and the water quality and quantity also vary greatly. Thus, it is difficult to be treated as organic wastewater. Besides, if the refractory substances (most of them have strong toxicity and "three causes") in pharmaceutical wastewater are discharged into water directly, they will remain in water for a long time, and accumulate and enrich the food chain, eventually enter the human body and endanger human health (Coimbra et al, 2019, Ferrer-Polonio et al, 2020, Hofman-Caris et al, 2017, Wang et al, 2020a). Therefore, efficient methods to treat pharmaceutical wastewater are sought continuously to reduce the harm of wastewater.

At present, many methods are provided to treat pharmaceutical wastewater, including biological

degradation (Mucha and Kułakowski, 2016, Zou et al, 2015), adsorption (Aniszewski, 2020, He et al, 2019), membrane separation (Ahsani et al, 2020, Chen et al, 2020, Guo et al, 2020, Urbanowska and Kabsch-Korbutowicz, 2019), advanced oxidation techniques (Dong et al, 2020, Khan et al, 2020, Klancar et al, 2016, Mukimin et al, 2020, Verma et al, 2013), new environmental materials method (Dong et al., 2020, Li et al, 2020, Lu et al., 2019) and so forth. Among them, the biodegradation has advantages of low consumption, high efficiency and low cost, while it has strict requirements on the concentration of influent. Accordingly, the biological technology cannot directly treat wastewater with high concentration of organic substances. Even if it can be processed, the processing conditions are very harsh. The operation of adsorption is simple, but the cost of most adsorbents is very high, and the regeneration of adsorbents is difficult. In the treatment of membrane separation, pollutants are easy to remain on the membrane and cause membrane fouling. Besides, there are fewer types of membrane materials, so the performance of wastewater treated is unstable (Phoon et al, 2020). The advanced oxidation, which attracts people's attention these years due to its high efficiency, no secondary pollution, wide range of application and easiness to control, is a technology which

produces hydroxyl radical (OH) with strong oxidation ability under the reaction conditions of high temperature and high pressure, electricity, sound, light irradiation, and catalyst. By utilizing the advanced oxidation technology, the refractory organic substances of macromolecules could be oxidized into low toxic or non-toxic small molecular substances. Schrank et al. use diverse advanced oxidation techniques of UV (Ultraviolet Light), TiO_2/UV, O_3 and O_3/UV to degrade pollutants in tannery wastewater; it demonstrates that the biodegradation of wastewater is enhanced through oxidation, and the toxicity of pollutants is also decreased (Schrank et al, 2004). Hofman-Caris et al. removed pharmaceuticals from wastewater effluent and dissolved non-biodegradable organic matter by advanced oxidation technique. The results suggest that advanced oxidation techniques could remove multiple different pharmaceuticals and humic acid to a large extent (Hofman-Caris et al., 2017).

Wet air oxidation (WAO) technology is a kind of advanced oxidation technology. It can oxidize organic substances in wastewater to small molecules or inorganic matter under the condition of high temperature (120–320°C) and high pressure (0.5 ~20 MPa). Gaseous oxygen is utilized as oxidant in this reaction. Moreover, it can treat wastewater with refractory substances, and be highly evaluated by many researchers due to its simple operation and easy industrialization. However, the WAO technology requires high temperature, and the cost to treat wastewater is very high. To solve this problem, the existing idea is to add suitable catalysts on the basis of WAO, which calls catalytic wet air oxidation (CWAO), so that the reaction could be carried out under mild conditions. In this way, it could reduce the cost of wastewater treatment, and improve the removal efficiency (Kang et al, 2011).

The development of catalysts is crucial to the treatment of pollutants in catalytic wet oxidation technology. So far, the research of catalytic wet oxidation has focused mainly on the synthesis of novel catalysts and investigating the effect of materials on wastewater treatment in CWAO. Researchers have developed a series of catalysts in CWAO, such as TiO_2 (Lunagomez Rocha et al, 2015), Al_2O_3 (Sushma et al, 2018), CeO_2 (Parvas et al, 2019), MoO_3 (Li et al, 2009, Wang et al, 2017, Wang et al, 2020b) and so on. Among them, MoO_3 exhibits favorable catalytic performance in the degradation of organic pollutants. Li et al. synthesized one-dimensional Ce-doped MoO_3 nanofibers with different doping amounts by combining sol-gel method and electrospinning technology. It was found that 11.86wt% CeO_2-doped nanofibers exhibited excellent catalytic activity for the fast degradation of organic dye (Li et al., 2009). Wang et al. synthesized MoO_3 catalyst by hydrothermal method, and the catalytic material demonstrated good catalytic performance at 400°C for the degradation of dye wastewater (Wang et al., 2017). Wang et al. synthesized highly active and stable nano-hybrid bimetallic catalysts, and applied to the treatment of organic dyes and obtained excellent degradation efficiencies in catalytic wet air oxidation system (Wang et al., 2020b). This demonstrates that MoO_3 catalyst is a very effective and potential material in the field of wet air oxidation treatment of industrial wastewater. However, this research is insufficient in the following two aspects. Firstly, most of the wastewater used in studies is simulated wastewater,

while the practical wastewater used in research is relatively rare. The catalytic performances of MoO_3 synthetic materials in wet air oxidation of pharmaceutical production wastewater are also rarely reported. Secondly, these studies do not thoroughly analyze the degradation mechanism of catalysts for catalytic wet air oxidation of wastewater.

This study has made some supplements to these two aspects. We obtained practical wastewater from pharmaceutical companies to analyze the degradation effect of MoO_3 catalyst in CWAO. The organic pollutants produced in pharmaceutical wastewater are in large quantities, do great harm, and are difficult to be degraded due to their complex compositions. If MoO_3 catalyst could be applied to the wet air oxidation treatment of pharmaceutical wastewater, it would not only promote the application of MoO_3 catalytic material, but also provide a new choice of technique for the treatment of pharmaceutical wastewater, thus alleviate the harm of pharmaceutical wastewater to the environment. Also, with the aid of Density Functional Theory (DFT) calculations, we attempt to reveal the microscopic mechanism of MoO_3 as a catalyst to degrade pharmaceutical wastewater in CWAO through analyzing the energy band structure of material.

Hence, in this paper, MoO_3 catalyst is prepared and synthesized by hydrothermal synthesis methods. The synthetic material properties are fully characterized by liquid specific surface area analyzer, X-ray diffractometer (XRD), scanning electron microscope (SEM), thermogravimetric analyzer, and other modern and advanced analytical techniques. The synthetic catalyst is applied to degrade pharmaceutical wastewater by catalytic wet air oxidation. The impact of catalytic dosage, reaction temperature, and reaction time on the degradation of pollutants is investigated. In addition, the reaction process of catalytic wet air oxidation on the pharmaceutical wastewater is modeled by the first-order and second-order kinetic equation. The recycling of catalyst in wet air oxidation system is also discussed. Furthermore, to illustrate the catalytic mechanism of MoO_3 on the degradation of pharmaceutical wastewater, the band structure and Density of States (DOS) of catalyst were obtained through DFT calculation.

Experimental equipment and methods

Preparation of catalyst

The hydrothermal synthesis method is performed for the preparation of catalyst. The mixture of 56 g $(NH_4)_6Mo_7O_{24}\cdot4H_2O$ and KNO_3 was dissolved in distilled water at 70°C and fully mixed. Among the mixed liquor, the amount of KNO_3 was 5.1 g. To control the pH of solution, 0.1 mol/L HNO_3 and KOH solution was used to adjust the pH (range from 4 to 7). The solution was transferred to the KH-50 type hydrothermal synthesis reactor at 125°C for 24 h. The outer shell of the hydrothermal reactor was made of stainless steel, and the inner lining was made of polytetrafluoroethylene produced by Beijing Getimes Technology Co., Ltd. Then, the resulting precipitate was filtered and washed with deionized water at room temperature until the pH value of the filtrate reached 7. The mixture was then dispersed in the 450 ml acetone and mixed for 2.5 h. After that, the mixture was filtered, and the residue was collected and dried at 85°C for 16 h in the electro-

-thermostatic blast oven. The sample was ground and roasted in a muffle furnace at 430°C for 4 h. Finally, the catalytic material was obtained by naturally cooling at room temperature in the Carbolite muffle furnace.

Characterization of catalyst

The synthetic catalyst is characterized by liquid specific surface area analyzer, X-ray diffractometer, scanning electron microscope, Fourier transform infrared spectroscopy, thermogravimetric analyzer, X-ray photoelectron spectroscopy spectra (XPS), and so on. In this experiment, we used Xigo liquid specific surface area analyzer (XiGo Nanotools, USA) to measure the specific surface area of the catalyst, and evaluate the properties of synthetic material. The morphology and composition of the catalyst was determined by S-3400N II scanning electron microscope (Hitachi Company, Japan). The characteristic functional group structure, molecular structure and chemical composition of the catalyst are analyzed by Thermo Scientific Nicolet is 5 Fourier transform infrared spectroscopy (FTIR) using pressed KBr discs. Moreover, the image of the catalyst was analyzed by X'tra X-ray diffractometer (ARL Company of Switzerland). The thermoweight of the catalyst was measured by Pyris 1 DSC thermal analyzer (PerKinElmer Company, the United States). The X-ray photoelectron spectroscopy spectra were recorded on PHI 5000 VersaProbe XPS equipment. The UV-vis spectrum research was carried out by PerkinElmer Ultraviolet spectrophotometer.

Catalytic wet air oxidation

The experiment of catalytic wet air oxidation to treat the wastewater was carried out in GCF permanent magnet rotating stirred autoclave (Dalian automatic Control Equipment Factory, 0.5 L, China). The pharmaceutical wastewater of 100 ml was mixed with the catalyst, and put into a clean autoclave. Then, the lid of the kettle was placed on the kettle body according to the fixed position carefully, and the high pressure rotating stirred autoclave was sealed by hexagon nuts and flanges to maintain good air tightness of the reactor. After sealing, a certain oxygen partial pressure was maintained through an oxygen tank and high pressure resistant copper pipeline. After that, the mixed substances were heated to a set reaction temperature through adjusting heating voltage device, and then the catalytic reaction experiment of wet air oxidation for the pharmaceutical wastewater was carried out in the autoclave.

In the process of catalytic reaction, the reaction temperature was maintained constant, and the cooling water was used to reduce the reaction temperature of reactor body. At the end of the catalytic reaction experiment, the autoclave was naturally cooled to room temperature. Afterwards, the supernatant of mixtures was taken to the filtrating device for filtration, and the concentration of residual total organic carbon (TOC) and chemical oxygen demand (COD) were analyzed in the sample. The analysis of TOC was carried out by Metash TOC-3000 total organic carbon analyzer, and the value of COD was analyzed by the national standard 11914-89 chemical oxygen demand. In order to investigate the effect of catalytic wet air oxidation system on the treatment of pharmaceutical wastewater, the wet air oxidation system was compared in all experiments. The removal rate and the removal growth rate and average

degradation rate of COD or TOC were as follows (equation 1 to 6), respectively.

$$Removal_{COD} = \frac{COD_t - COD_0}{COD_0} \cdot 100\% \quad (1)$$

$$Removal\ growth\ rate_{COD} =$$
$$= \frac{Removal_{COD_n} - Removal_{COD_{n-1}}}{Removal_{COD_n}} \cdot 100\% \quad (2)$$

$$Average\ degradation\ rate_{COD} = \frac{Removal_{COD_t}}{t} \quad (3)$$

where:
$Removal_{COD}$ is removal rate of COD (%); COD_0 is original COD concentration (mg/L);
COD_t is COD concentration at reaction time t;
Removal growth rate is a parameter to evaluate the effect of catalyst dosage or reaction temperature on removal efficiency (%);
$Removal_{CODn}$ is a COD removal rate at a certain catalyst dosage or reaction temperature; $Removal_{CODn-1}$ is a COD removal rate at the previous catalyst dosage or reaction temperature; *Average degradation rate* is a parameter evaluates the average removal efficiency over a period of reaction time; t is reaction time.

$$Removal_{TOC} = \frac{TOC_1 - TOC_0}{TOC_0} \cdot 100\% \quad (4)$$

$$Removal\ growth\ rate_{TOC} =$$
$$= \frac{Removal_{TOC_n} - Removal_{TOC_{n-1}}}{Removal_{TOC_n}} \cdot 100\% \quad (5)$$

$$Average\ degradation\ rate_{TOC} = \frac{Removal_{TOC_t}}{t} \quad (6)$$

where:
$Removal_{TOC}$ is removal rate of TOC (%); TOC_0 is original TOC concentration (mg/L); TOC_t is TOC concentration at reaction time t;
Removal growth rate is a parameter to evaluate the effect of catalyst dosage or reaction temperature on removal efficiency (%);
$Removal_{TOCn}$ is a TOC removal rate at a certain catalyst dosage or reaction temperature;
$Removal_{TOCn-1}$ is a TOC removal rate at the previous catalyst dosage or reaction temperature;
Average degradation rate is a parameter which evaluates the average removal efficiency over a period of reaction time; t is reaction time.

To investigate the influence of reaction parameters on the degradation effect of wastewater in CWAO, a series of experiments were performed which evaluated the impact of catalytic dosage, reaction temperature, and reaction time

on the removal efficiency of pollutants. The TOC and COD values of raw pharmaceutical wastewater were 7660 mg/L and 7490 mg/L, respectively. The catalytic dosage was from 0 to 6.0 g/L, the reaction temperature was from 145°C to 220°C, and the reaction time was from 0 to 4.0 h. In the course of experiments, the initial partial pressure of oxygen was maintained at 1.4 MPa. To better evaluate the effect of CWAO at different reaction parameters, experiments at similar conditions in WAO were conducted as comparison.

The recycle of catalyst

To evaluate the stability and activity of synthesis catalyst, experiments of the catalyst reuse were performed in our laboratory. After the catalytic reaction of wet air oxidation for pharmaceutical wastewater, the solid and liquid in the mixture were separated by a filtration device using circulating pump. Then, the solid material was washed several times with distilled water until it was neutral. After that, the solid sample was collected and dried at 85°C for 16 h in the electro-thermostatic blast oven. The reaction conditions were as follows: the reaction temperature was 190°C, the catalyst dosage was 2.0 g/L, the partial pressure of oxygen was 1.4 MPa, and the reaction time was 2.5 h. In this experiment, the catalyst was reused three times. The microscopic morphology and mineral phase of catalyst were also evaluated after recycling.

DFT calculation

To further reveal the internal reaction mechanism of the catalyst in wet air oxidation for pharmaceutical wastewater, the band structure and density of states (DOS) of the catalyst were calculated. The density functional theory calculation process was carried out with Vienna Ab initio Simulation Package (VASP) (Kresse and Furthmuller, 1996) and spin-polarized density function theory. Perdew-Burke-Ernzerhof (PBE) functional (Hohenberg and Kohn, 1964, Kohn and Sham, 1965) within the generalized gradient approximation (GGA) (Perdew et al, 1996, Perdew et al, 1992) method was used to calculate the exchange-correlation potential. The hybrid functional method was used to calculate the energy band. The cut-off energy for the calculation iwass 450 eV. The K-points grids of dimensions were 5×5×5. Both the atomic coordinates and cell parameters of MoO_3 were optimized. The theoretical MoO_3 model structure was a cell unit including 4Mo and 12O atoms, as shown in Fig. 1a. The Surface model for calculating work function is shown in Fig. 1b and the vacuum slab was set as 30Å.
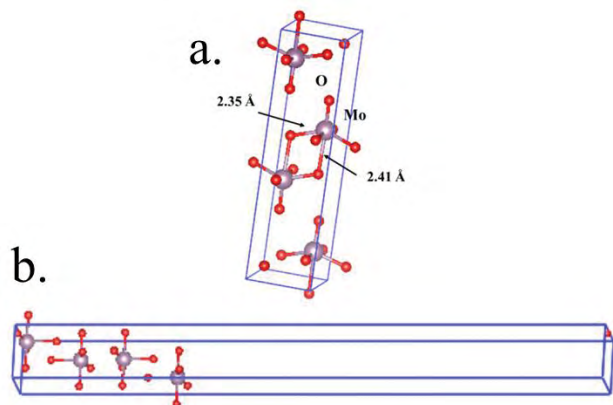
Results and discussion

Solution specific surface area

The specific surface area of the catalyst is an important indicator used to measure the performance of the catalyst. The larger the specific surface of catalyst, the larger the molecular contact area with the reacting substance, which could accelerate the activity of the catalyst to a certain extent. The measurement results of liquid specific surface for the catalyst are depicted in Fig. 2. Through the fitting and calculation of instrument software, the solution specific surface area of the catalyst in the experiment is 468 m^2/g. In our previous research, the liquid specific surface of the synthesized catalyst which used γ-Al_2O_3 as a carrier was about 350 m^2/g (Chen et al, 2018). Also, two kinds of catalyst were synthesized and used in wet air oxidation, and the liquid specific surfaces of them ranged from 360 m^2/g to 440 m^2/g (Chen et al, 2019b). These findings suggest that the catalyst synthesized in this study could provide sufficient specific surface area during the catalytic reaction.
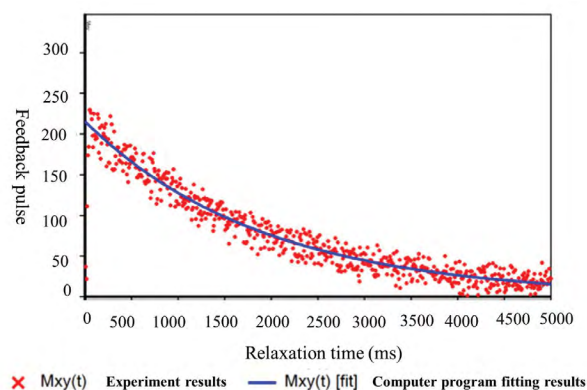

Fig. 2. Solution specific surface area of catalyst

XRD

Fig. 3 depicts the X-ray diffraction pattern of the catalyst, which shows that the main mineral phases of synthetic product are α-MoO_3 (abundant) and h-MoO_3 (little). The α-MoO_3 diffraction peaks can be found at around 2θ: 12.76, 23.32, 25.68, 27.35, 33.66, 38.96, 45.78, and 49.24°, respectively. The other diffraction peaks, including only 9.31 and 28.76, belong to h-MoO_3. This XRD findings are akin to other paper (Ma et al, 2015) that suggests α-MoO_3 (mixed with a little h-MoO_3) is successfully synthesized in the experiment.

Fig. 1. The crystal structure of MoO_3 catalyst
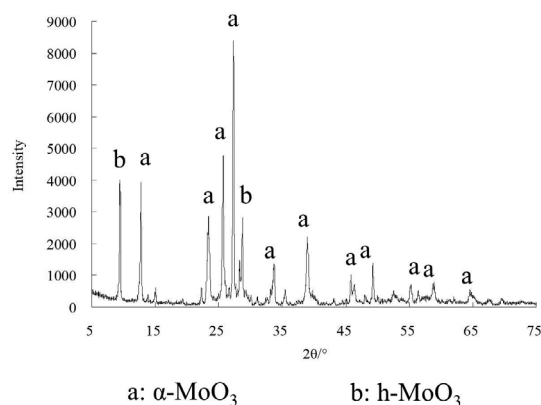

a: α-MoO_3 b: h-MoO_3

Fig. 3. XRD pattern of catalyst

FT-IR

Fig. 4 shows the analytical results of FT-IR for synthetic material. The main FT-IR absorption peaks appear at 1392, 992, 957, 894, and 606 cm^{-1}. The peaks at 1392 cm^{-1} belong to the bond of H-O, which could be caused by adsorbed water left in the catalyst (Chen et al, 2012, Cheng et al, 2018). All the other peaks, including 992, 957, 894, and 606 cm^{-1}, might belong to the bonds of Mo-O (Wang et al., 2017) in α-MoO$_3$ and h-MoO$_3$. This indicates, in addition to the water adsorption, that the main groups of material are composed of O and Mo bonds. Consequently, the analytic result of FT-IR is consistent with that of XRD. These findings confirm that the α-MoO$_3$ and h-MoO$_3$ were successfully synthesized in our experiment.
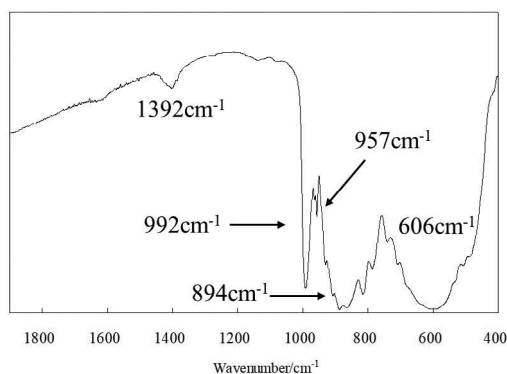

Fig. 4. FT-IR result of catalyst

SEM-EDX

To detect the microstructure and microelement composition of the reaction products, the sample was analyzed by SEM-EDX, and the analytic results are depicted in Fig. 5.

From Fig. 5a to Fig. 5d, we observe that most of the catalytic product has quadrangular prism like morphology. Besides, the length, width and thickness of catalyst crystal are around 5 μm, 2 μm, and 1 μm, respectively. The morphology of the catalyst is similar to that of other reference (Huang et al, 2010), and the crystal might be α-MoO$_3$ with orthorhombic cell structure. Fig. 5e and Fig. 5f show the wide range of EDS analysis results. It can be seen that the main chemical compositions of the catalyst are 20% Mo, 63.4% O, and 2.15% K (mass of atomic/%). Such analysis results are basically in line with the molecular composition of α-MoO$_3$, XRD, and FT-IR analysis results. Moreover, the little K element may come from the synthesis process of the catalyst.

Fig. 6 depicts the results of EDS element mapping of the catalyst. From the element distribution of Mo (Fig. 6b), the distribution position of Mo element is exactly the same as the position where the catalyst particles appear (Fig. 6a). In addition, compared with Mo element, the distribution of O element (Fig. 6c) is relatively loose. However, it is also basically distributed in the position where the catalyst material particles appear (Fig. 6a), which further verifies that the material is MoO$_3$ crystal. Moreover, the intensity of K element distribution points in Fig. 6d is far inferior to that of Mo and O,
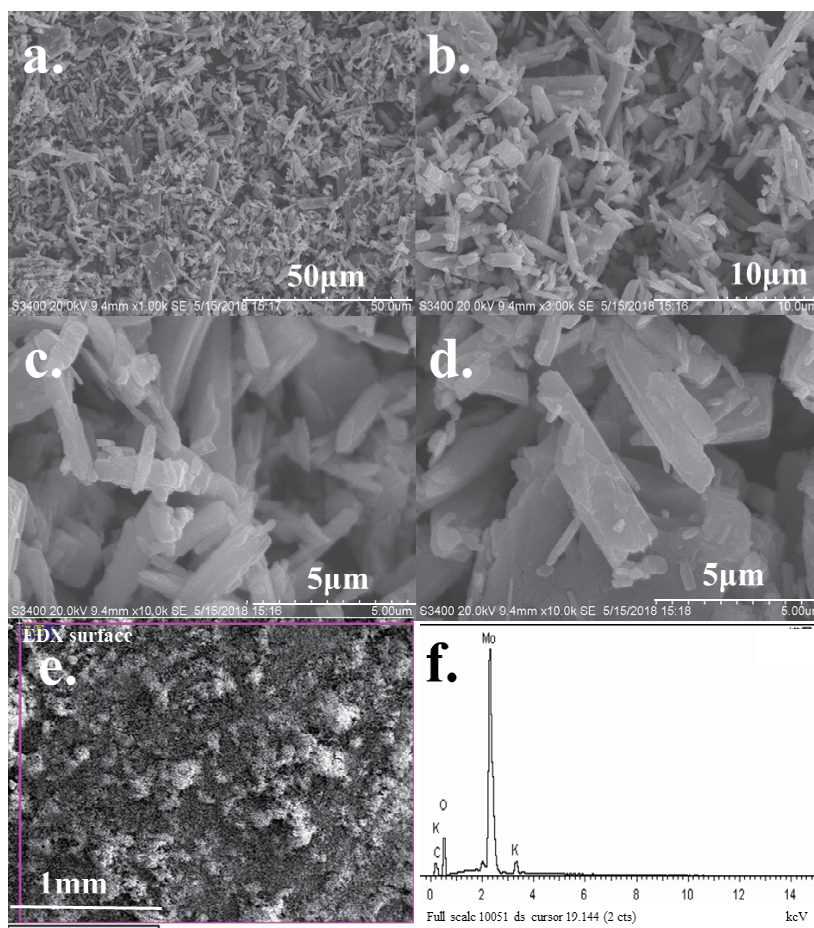

Fig. 5. SEM-EDS analysis results of catalyst

which indicates that the catalyst contains only trace amounts of K element. These findings are consistent with the results of EDS analytical results. Furthermore, according to the related references (Zhang et al, 2016), the catalytic performance of α-MoO$_3$ could be increased by mixing with K, Na, and other alkali elements in the catalyst.

TG-DTG

To detect the thermal effect of the synthesized material, the sample was analysed by TG-DTG instrument. Fig. 7 describes the TG and DTG analytical results of the catalyst under the condition of N$_2$. As the temperature rises from room temperature to 700°C, the mass loss of catalyst is only 1.5%. In addition, the DTG curve only appears very small values ranging from room temperature to 100°C, and from 530°C to 600°C, respectively. These results indicate that the α-MoO$_3$

catalytic product has favorable thermal stability, which is very suitable as a high temperature catalyst.

XPS

XPS characterization results are exhibited in Fig.8 which depicts the full spectrum of MoO$_3$ catalyst. All characteristic peaks of MoO$_3$ are observed, including Mo 3d (232 eV), Mo 3p 3/2 (397 eV), Mo 3p 1/2 (414 eV) and O (530 eV). These findings are in accord with other characterization results for the catalyst, and further prove the chemical composition of MoO$_3$ catalyst (Huang et al., 2010, Li et al., 2009). The more details can be found from the high-resolution XPS spectra of Mo 3d (Fig. 8b), which depict two characteristic peaks which are detected at 231 eV and 234 eV. They should belong to Mo 3d 2/5 and Mo 3d 2/3, respectively. Moreover, the negative binding energy shift might be explained to the bonds
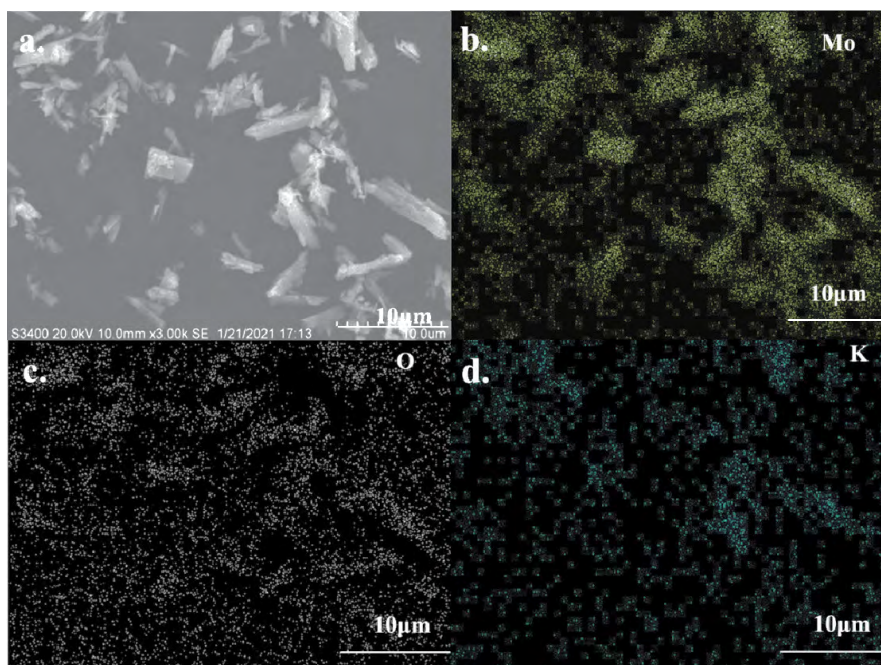

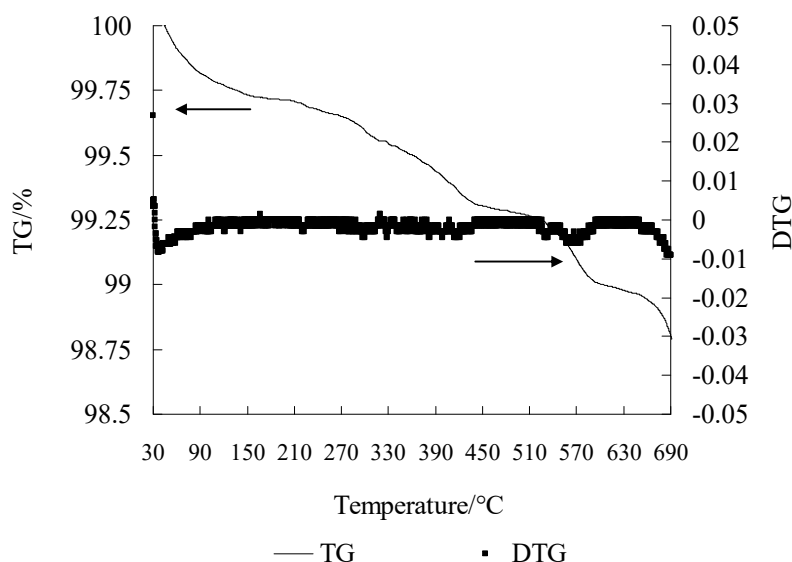**Fig. 6.** EDS element mapping analysis results of Mo (b), O (c) and K (d)

Fig. 7. Thermo-gravimetric analysis results of catalyst (N$_2$ condition)

between O and Mo (Wang et al., 2017, Wang et al., 2020b). Besides, further peak splitting analysis states that both the characteristic peaks at 231 eV and 234 eV are composed of two small peaks at 235 eV and 232 eV (pink line), 234.5 eV and 231.5 eV (blue line). The detection results should be caused by the presence of two Mo-O bonds in MoO_3 catalyst. Fig.8c shows the high-resolution XPS spectra of O1s. For similar reasons as for Mo 3d, the peak of O 1s at 530 eV also can be divided into two small peaks at 529.5 eV (blue line) and 531 eV (pink line).

Effect of catalyst

The effect of catalyst doses on the removal rate of TOC and COD is shown in Fig. 9. It is obvious that the removal rates of TOC and COD for pollutants are promoted in CWAO after adding the catalyst. In addition, there is a rapid increase when
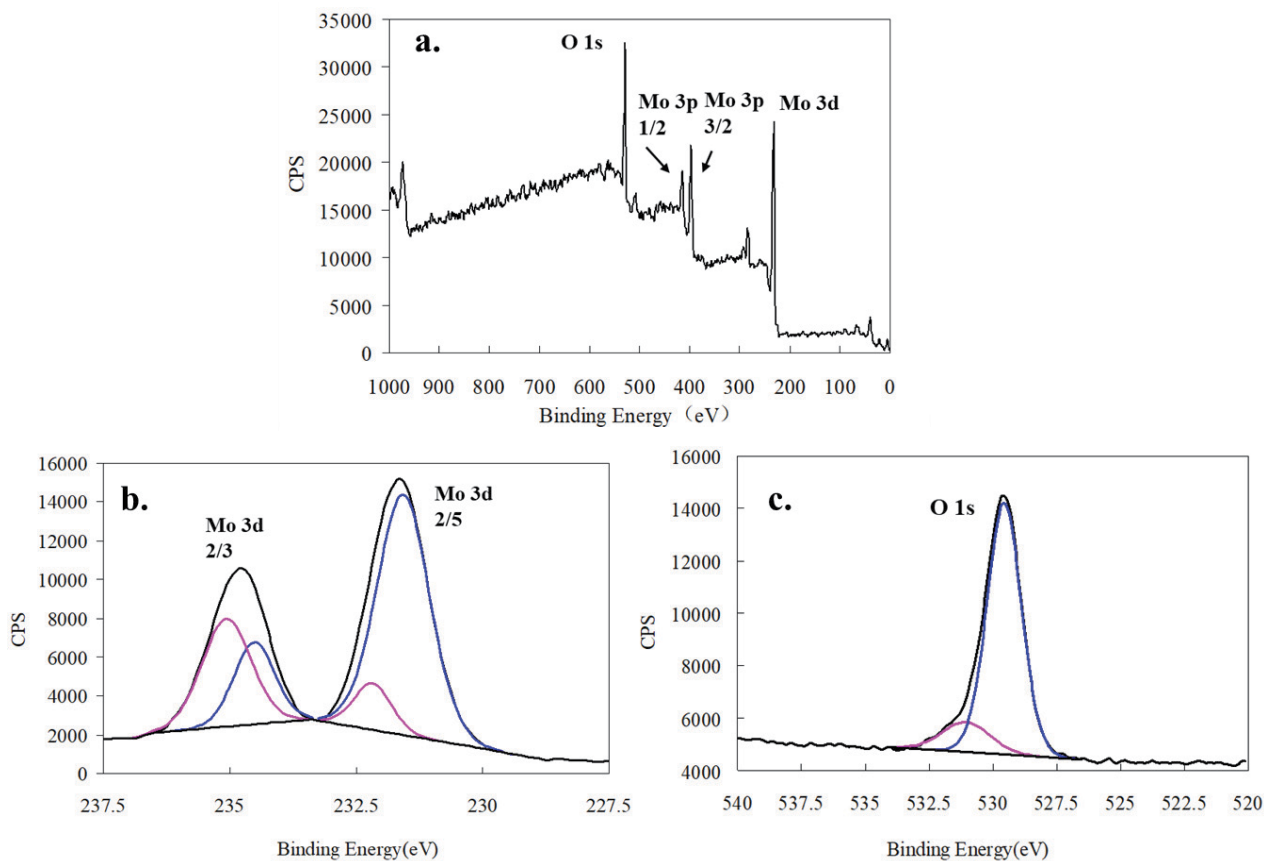

Fig. 8. (a) the wide scan XPS spectra of MoO_3 catalyst; (b) and (c) the high-resolution XPS spectra of Mo 3d and O 1s
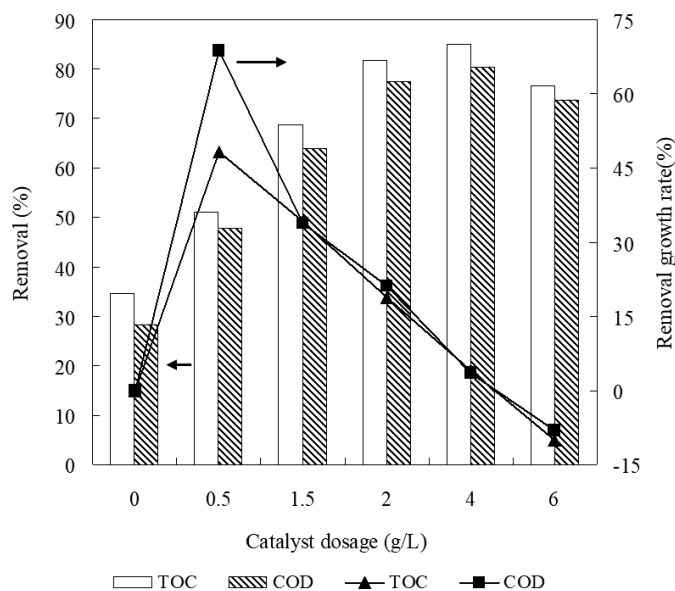

Fig. 9. Effect of catalyst dosage on TOC and COD removal (reaction temperature: 175°C; reaction time: 2.5 h)

the catalyst dosages range from 0 to 4.0 g/L. For instance, when the catalyst dose is 4 g/L, the removal rates of TOC and COD in CWAO system are up to 85.09% and 80.31%, respectively, i.e., more than 50% higher than those of systems with no catalyst. However, when the catalyst dosage is further increased to 6.0 g/L, the TOC and COD removal rate are slightly decreased, indicating that too much catalyst is not conducive to the catalytic reaction in CWAO. Excessive catalyst might hinder the diffusion of oxygen in solution, impact the removal rate of TOC and COD, and thus decrease the degradation efficiency of pollutants in wastewater. Moreover, the removal growth rates of TOC and COD were calculated in this study. When the catalytic dose was 0.5 g/L, the removal growth rates of TOC and COD were up to 0.4823 and 0.6877, respectively, whereas it decreased gradually with the increase of catalyst doses. Accordingly, considering the removal effect of pollutants and the economy of catalyst dosage in CWAO reaction, the adding amount of catalyst was 2.0 g/L in the following experiments.

Effect of reaction temperature

The reaction temperature is a decisive factor that influences the degradation effect of wastewater in WAO (Yadav et al, 2016). Fig. 10 depicts TOC and COD removal rates in CWAO at different reaction temperatures. The reaction time is 2.5 h. It is discovered that, the reaction temperature has a significant impact on the degradation of pollutants in CWAO. With the increase of reaction temperature, the removal efficiencies of TOC and COD are enhanced continually. When the optimal reaction temperature is 220°C, then the TOC and COD removal rates are up to 97.43% and 93.46%, respectively. Besides, the TOC and COD removal rates in CWAO system are more than 40% higher than those in WAO system (the TOC and COD removal rates are 46.82% and 41.54%, respectively). We also investigated the removal rates of pollutants at 230°C, and there was no significant increase in the removal rates of TOC and COD. In addition, it can be seen from the figure that, when the temperature grows from 160°C to 175°C, the removal efficiencies of COD and TOC in CWAO are greatly increased. Moreover, the removal growth rates of TOC and COD are up to 0.5321 and 0.5712 at 160°C, respectively. As

the reaction temperature is greater than 160°C, the solubility of water increases, and the viscosity of liquid decreases with the increase of temperature. Accordingly, it is beneficial to the mass transfer of oxygen in liquid, and favorable to the degradation of pollutants, thus enhances the removal rate of pollutants.

Effect of time and reaction kinetics

The influence of reaction time on TOC and COD removal rates are depicted in Fig. 11. The reaction temperature is 175°C. The reaction time is also fundamental to the removal of pollutants. We observe that there is a steady rise for TOC and COD removal rates together with the increase of reaction time. The TOC and COD removal rates at reaction time of 4 h in CWAO are up to 86.12% and 82.27%, respectively. The average removal rates of TOC and COD at different reaction time are calculated simultaneously in Fig. 11. The curves state that TOC and COD average removal rates are decreased gradually, and they achieve the highest at the reaction time of 0.25 h. These findings indicate that, by extending the reaction time, the removal of pollutants can be improved to a certain extent. However, it might be limited with further prolongation of reaction time.

To further investigate the removal process of pollutants in CWAO, the kinetic equations are utilized to evaluate the reaction process. The first-order kinetic and the second-order kinetic equations are used to model (Chen et al, 2019a, Zhang et al, 2020) the reaction process at different reaction times in CWAO and WAO systems, and the fitting results are shown in Table. 1. From the fitting results of the first order kinetic equation, the fitting R^2 values of TOC and COD in CWAO are only 0.8433 and 0.8328, respectively, whereas the R^2 values of the second order kinetics are up to 0.9634 and 0.9786, respectively. These fitting data state clearly that the second order kinetics could better model the degradation process of pollutants in CWAO system. Moreover, a similar result was obtained in WAO system.

Effect of catalyst recycling

To further evaluate the catalytic performance of MoO_3, the experiments were carried out to investigate the degradation effect of TOC and COD as catalyst recycling, and the
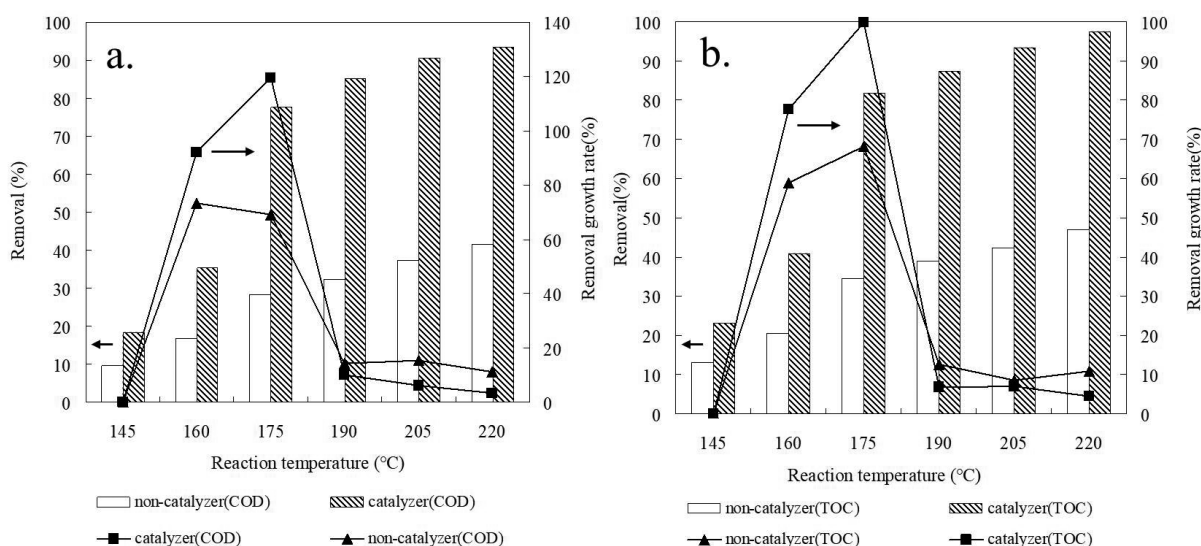

Fig. 10. Effect of reaction temperature on COD and TOC removal (catalyst dosage: 2.0 g/L, reaction time: 2.5 h)

morphology of catalyst after reuse was also studied, as shown in Fig. 12. The MoO_3 catalyst was recycled three times in this experiment. Fig. 12a and Fig. 12b show the SEM analysis results of the catalyst after three cycles of reuse. After 3 cycles of use, the catalyst still maintained a rod-like crystal structure, and its microscopic size was basically the same as that of the original catalyst, which indicates that the main composition and structure of the catalyst remained stable. However, the surface of the rod-shaped crystal material (Fig. 12b) changed from smooth (Fig. 5c and Fig. 5d) to rough compared with the original catalyst. This indicates that the surface structure of the catalyst has changed during the catalytic wet air oxidation process. Fig. 12c depicts the XRD diffraction results of the catalyst after three cycles of reuse. Similar to the result of SEM, the peak position of XRD diffraction after recycling is exactly the same as that of the initial catalyst. This also implies that the main structure of material is basically stable. Nevertheless, compared with the original XRD result in Fig. 3, the intensity of the peak at each peak position has decreased. This indicates that the crystallization degree of the material decreases with the

progress of reaction in catalytic wet air oxidation system. This may be largely related to changes in the surface of material.

Fig. 12d shows the effect of the catalyst recycling on the removal rate of TOC and COD. As the number of catalyst reuse increases, the removal efficiency of TOC and COD is weakened gradually. In addition, the catalytic effect is the best when the MoO_3 catalyst is used for the first time. Combined with the morphology analytical results of the catalyst, we speculate that the decrease of catalytical effect after recycling might be related to the change of microstructure surface and crystal crystallinity of the material. However, the removal rates of TOC and COD are still more than 60% after the catalyst is reused three times, which demonstrates that the MoO_3 exhibits a favorable reusability and catalytic stability in the application of CWAO.

The catalytic mechanism

It is believed that the catalytic material is in the state of thermal excitation at a high temperature in the process of catalytic wet air oxidation. In this situation, the band structure of catalytic
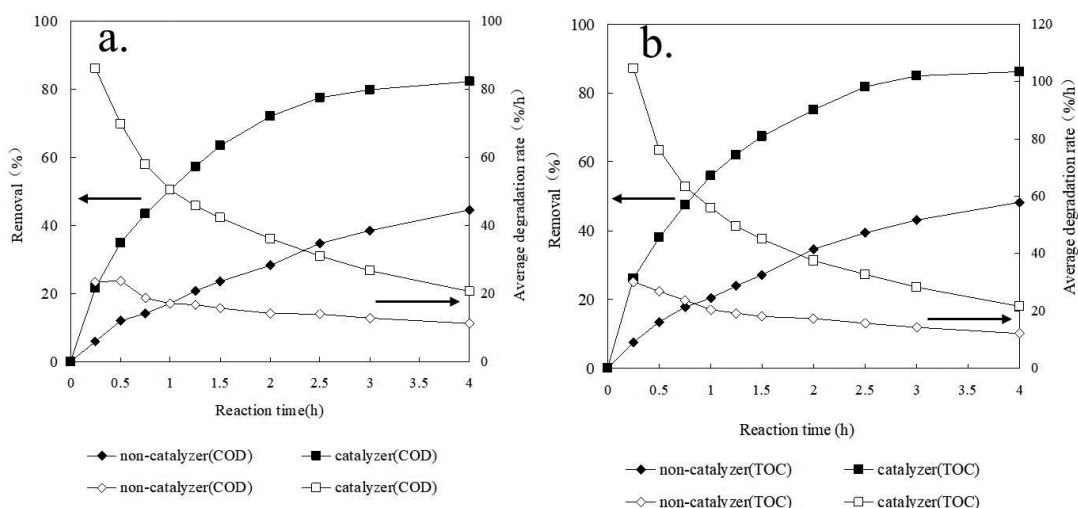

Fig. 11. Effect of reaction time on COD and TOC removal (reaction temperature: 175°C; catalyst dosage: 2.0 g/L)

Table 1. The kinetics fitting results

$Ln\dfrac{C_{COD_0}}{C_{COD_t}}=k_{COD}t \quad Ln\dfrac{C_{TOC_0}}{C_{TOC_t}}=k_{TOC}t$		**First-order-kinetics (Chen et al, 2014a, Chen et al, 2014b)**	
		k_1 (h⁻¹)	R^2
WAO	COD	0.1618	0.8623
	TOC	0.1883	0.8721
CWAO	COD	0.5377	0.8328
	TOC	0.6137	0.8433
$\dfrac{1}{C_{COD_0}}-\dfrac{1}{C_{COD_t}}=k_{COD}t \quad \dfrac{1}{C_{TOC_0}}-\dfrac{1}{C_{TOC_t}}=k_{TOC}t$		**Second-order-kinetics (Chen et al., 2014a, Chen et al., 2014b)**	
		k_2 (L.mg⁻¹.h⁻¹)	R^2
WAO	COD	0.000024	0.9959
	TOC	0.000027	0.9891
CWAO	COD	0.0001438	0.9786
	TOC	0.00018	0.9634

materials is very important for the catalytic effect. UV-visible (UV-vis DRS) diffuse reflection is a common method to study the band gap of materials. The UV-vis DRS results of MoO_3 catalyst are displayed in Fig.13a. It suggests that the main light absorption range of MoO_3 catalyst is from about 300 nm to 420 nm. Based on the data of Fig.13a, the Tauc equation (as bellow) is often used to calculate the band gap energy.

$$\alpha(v)hv = A(hv - Eg)^{n/2} \qquad (7)$$
$$\text{(Dong et al., 2020, Khan et al., 2020)}$$

Where, α, h, v, A and Eg represent absorption coefficient at light frequency v, Planck constant, light frequency, a constant and band gap energy, respectively. For indirect transition semiconductor as MoO_3, the value of n is 2.

According to Tauc equation, the value of Eg could be obtained through plotting the curve of $[a(v)hv]^2$ versus hv and extra-polating the linear part of the curve to zero absorption coefficient. This analysis process is carried out and the results are depicted in Fig. 13b. It can be seen that the band gap energy of MoO_3 is 3.12eV, which is very close to the results of presented in the literature (Huang et al, 2014, Xu et al, 2020).

At present, DFT is an effective method to study the electronic structure of materials. Fig. 14a and Fig. 14b show the calculation results of energy band structure and the density of states DOS for the catalyst (MoO_3) material. The calculated band gap value is about 2.58 eV, which is smaller than the experimentally determined result (3.12 eV). This phenomenon is mainly caused by recognized defects in the calculation of density functional theory, and such errors are generally acceptable (Cheng et al, 2021). In addition, the
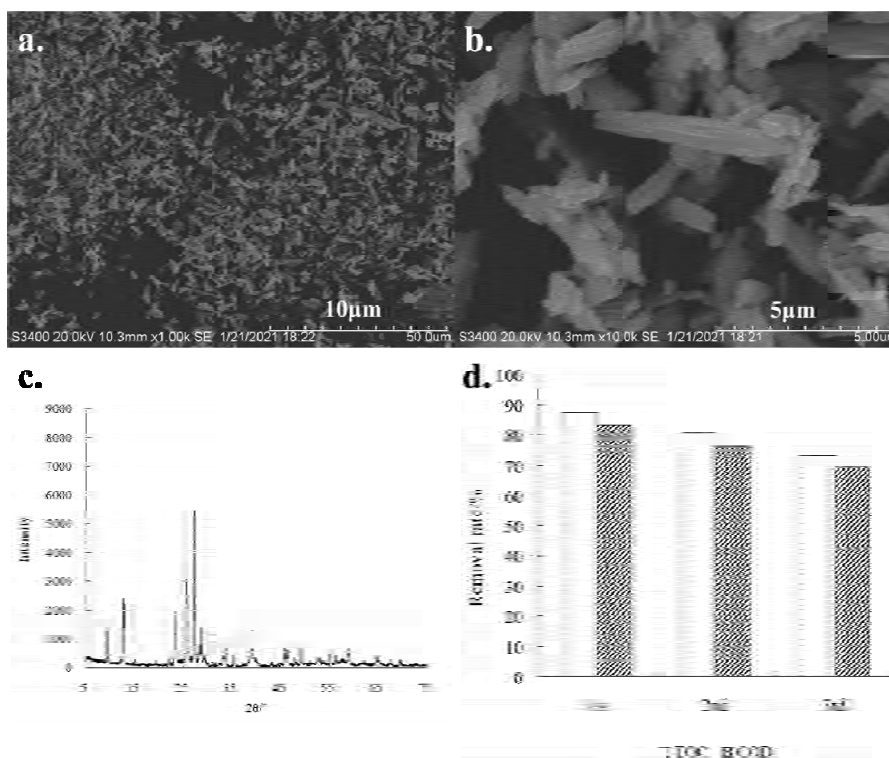

Fig. 12. (a) and (b) SEM analysis results of catalyst after three times of recycling; (c) XRD pattern of catalyst after three times of recycling; (d) Effect of catalyst recycling on the removal rate of TOC and COD
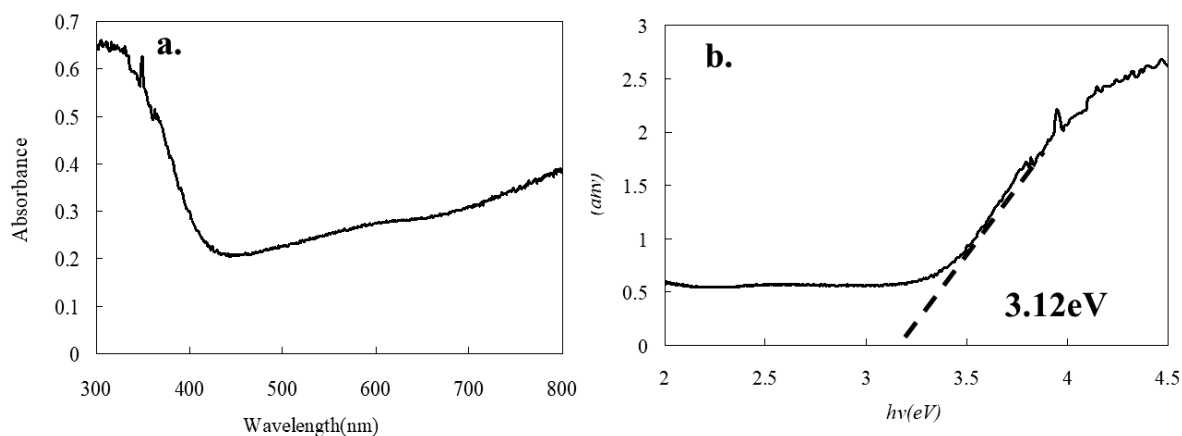

Fig. 13. UV-vis diffuse reflectance spectra of MoO_3 catalyst

highest point of the valence band for the catalyst material energy band structure is at point R, and the lowest point of the conduction band is at point Γ. Consequently, the catalyst material is a typical indirect band gap semiconductor. Fig. 13c shows the calculation results of the work function. It can be seen from Fig. 14c that the Fermi level energy is -2.47 eV, and the vacuum level energy is 1.4 eV. Therefore, the work function of MoO₃ is 3.87 eV, which suggests that the free electrons near Fermi level need energy of 3.87 eV to escape to the catalyst surface. Besides, the high temperature environment between 145°C to 220°C is sufficient to provide such thermal excitation energy. Similar to light excitation, the thermal excitation is also a common method for exciting semiconductor materials. Based on the DFT calculated results and the theory of semiconductor physics, we can approximately calculate the relationship between the number of thermally excited electrons (holes) and the absolute temperature. The main calculation formula is as follows

$$N_c = \frac{1}{4\pi^3}\left(\frac{2\pi m_c * k_B T}{\hbar^2}\right)^{\frac{3}{2}} \tag{8}$$

where:
N_c is the effective energy level density of conduction band. $\hbar$ is reduced Planck constant and the value is 1.05457266×10^{-34} J·s ($6.582119514\times10^{-16}$ eV·s).
k_B is Boltzmann constant and the value is 1.380649×10^{-23} J/K.
T is absolute temperature. m_e* is the conduction band effective mass of electronic.

$$n = N_c e^{-(E_c-E_F)/k_B T} \tag{9}$$

where:
n is the number of conduction band electrons.
E_c is energy at the bottom of conduction band (eV).
E_F is the energy of Fermi level.

$$N_V = \frac{1}{4\pi^3}\left(\frac{2\pi m_{hc} * k_B T}{\hbar^2}\right)^{\frac{3}{2}} \tag{10}$$

where:
N_v is the effective energy level density of conduction band.
m_h* is the valence band effective mass of hole.

$$P = N_V e^{-(E_c-E_F)/k_B T} \tag{11}$$

where:
P is the number of valence band holes.
E_g is energy at the top of valence band (eV). E_F is the energy of Fermi level.
For intrinsic semiconductors, the number of valence band holes is equal to the number of conduction band electrons.

$$n = p = \sqrt{N_c N_V} \cdot e^{-E_g/2k_B T} \tag{12}$$

$$E_g = E_c - E_V \tag{13}$$

According to the theory of solid energy band, the energy distribution of electrons and holes in a semiconductor
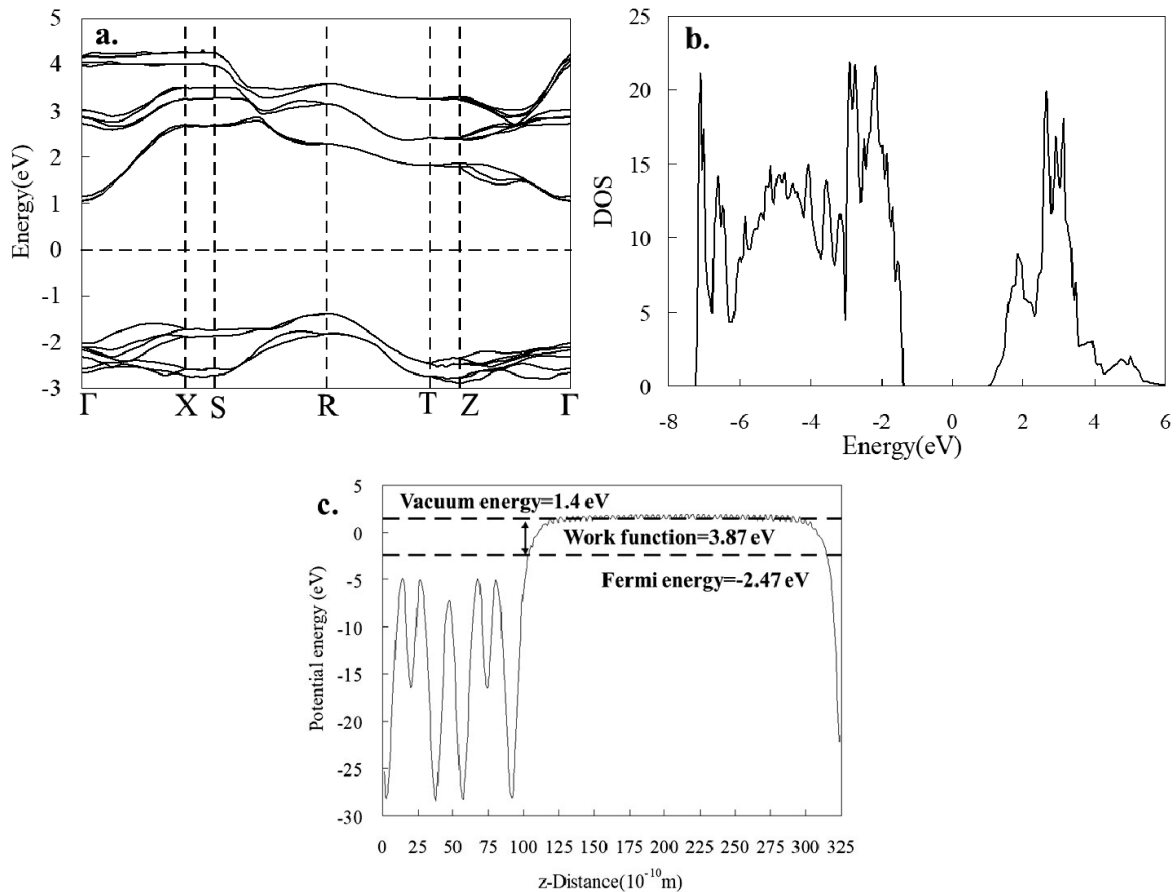

Fig. 14. The band structure (a), DOS (b) and work function (c) of MoO₃ catalyst gained from DFT calculation

conforms to the classic Boltzmann distribution. Once the ambient temperature is above absolute zero, electrons with valence bands are excited to the conduction band to form free electrons. At the same time, free holes are formed in the valence band. Besides, with the increase of excitation temperature, the number of free electrons and holes increases exponentially. The relationship between the number of free electrons (free holes) and the absolute temperature is shown in Fig. 15. It is clear that the number of conduction band free electrons (valence band free holes) increases with the ambient temperature growing. The relationship is expressed as an obvious exponential distribution. These findings indicate that the catalytic capability of MoO_3 could be enhanced by increasing the reaction temperature. It could be speculated that the free electrons excited to the conduction band can directly reduce the pollutants, or react with the O_2 in the system to produce $\cdot O^-$ radicals to degrade the pollutants. Furthermore, the free holes produced in the valence band can directly oxidize the pollutants, or they could also react with the gaseous H_2O to produce $\cdot OH$ radicals to degrade pollutants. It can also be seen

from Fig.16 that the number of conduction band free electrons can be clearly observed only as the ambient temperature is higher than about 430 K (157°C). Therefore, its catalytic activity should be higher than 430 K before it can be clearly displayed, and this phenomenon is in better agreement with the previous experimental results.

Conclusions

The catalyst of MoO_3 is prepared, fully characterized, and applied to the degradation of pharmaceutical wastewater in CWAO. The MoO_3 is successfully synthesized, which can be proved by the analytic results of FT-IR, XRD, SEM, and XPS characterization. In addition, the catalyst displays a favorable thermal stability. MoO_3 catalyst exhibits remarkable catalytic performance, and it greatly enhances the degradation efficiencies of pollutants in CWAO. The removal rates of pollutants are up to 93% at 220°C. The influence factors, including catalytic dosages, reaction temperature, and reaction time, have a great impact on TOC and COD removal rate.
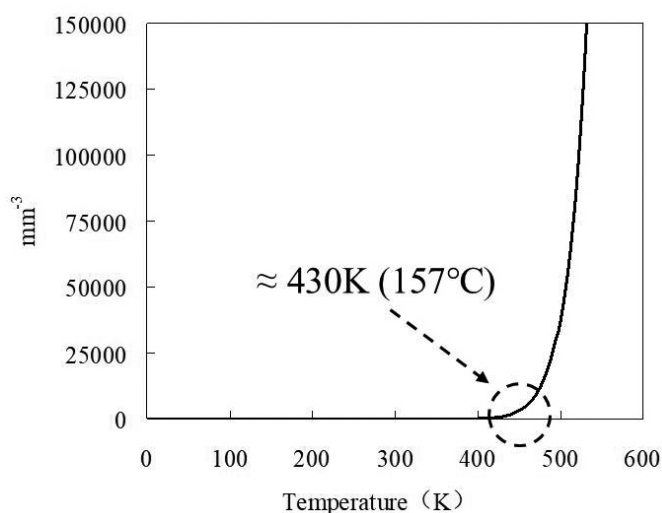

Fig. 15. The relationship between the number of thermally excited electrons (holes) and the absolute temperature in theory
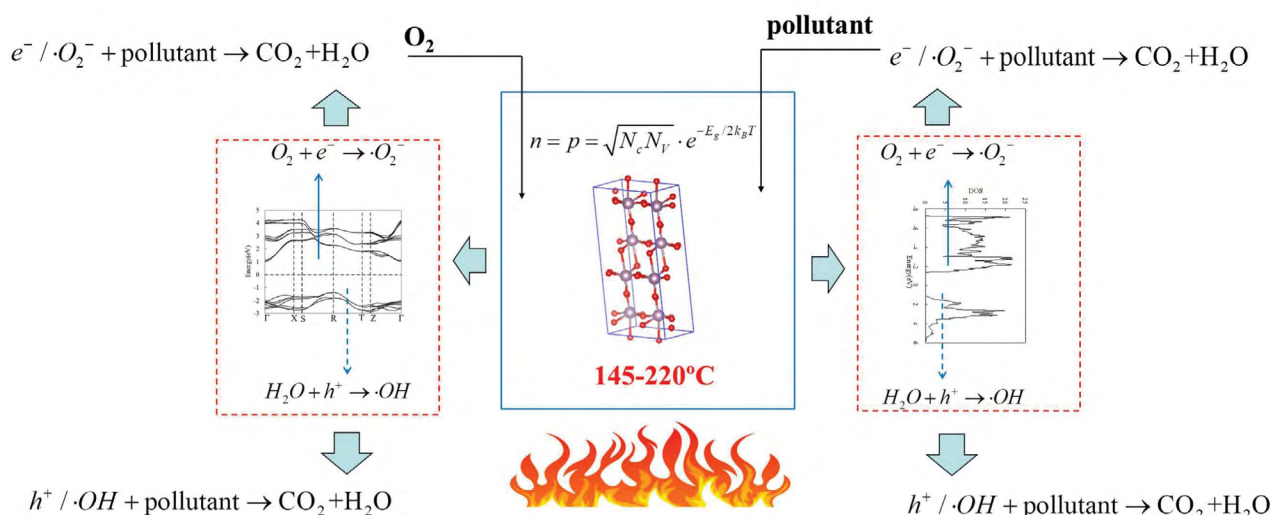

Fig. 16. The catalytic mechanism of MoO_3 catalyst

Besides, adding the catalyst in a proper range largely promotes the removal of pollutants, while excessive catalyst doses are not favorable to the degradation in CWAO. Moreover, with the increase of reaction temperature and reaction time, the degradation effect of pollutants is enhanced gradually, whereas the average removal rates of TOC and COD decrease continuously. The degradation process is better described by the second-order kinetics. After consecutive three time cycle, the catalyst is maintained stable in the degradation of pollutants. Furthermore, the catalytic mechanism of MoO₃ in CWAO states that the experimentally determined band gap energy of MoO₃ is 2.73 eV, while the calculated value is 2.58 eV, which is acceptable. Additionally, the calculation of energy band structure and the density indicate that MoO₃ is a typical indirect band gap semiconductor, and the free electrons excited to the conduction band could directly reduce the pollutants in CWAO. Also, the thermal excitation energy provided by the high temperature benefits the free electrons to escape the material surface. Then, these free electrons are excited to the conduction band, and degrade the pollutants directly. These findings demonstrate that MoO₃ can be used as a favorable catalyst to degrade pharmaceutical wastewater in advanced oxidation technology.

Acknowledgements

References

Ahsani, M., Hazrati, H., Javadi, M., Ulbricht, M. & Yegani, R. (2020). Preparation of antibiofouling nanocomposite PVDF/Ag-SiO2 membrane and long-term performance evaluation in the MBR system fed by real pharmaceutical wastewater. *Separation and Purification Technology*, 249, 116938. DOI: 10.1016/j.seppur.2020.116938

Aniszewski, A. (2020). Impact of ground adsorption capacity on he change on the chemical composition of groundwater. *Archives of Environmental Protection*, 46, 2, pp. 35–41. DOI: 10.24425/aep.2020.133472

Chen, C., Cheng, T., Shi, Y. & Tian, Y. (2014a). Adsorption of Cu(II) from Aqueous Solution on Fly Ash Based Linde F (K) Zeolite. *Iranian Journal of Chemistry & Chemical Engineering – International English Edition*, 33, 3, pp. 29–35. DOI: 10.30492/IJCCE.2014.11328

Chen, C., Cheng, T., Wang, Z.L. & Han, C. H. (2014b). Removal of Zn2+ in aqueous solution by Linde F (K) zeolite prepared from recycled fly ash. *Journal of the Indian Chemical Society*, 91, 2, pp. 285–291 https://www.researchgate.net/publication/295591718_Removal_of_Zn2_in_aqueous_solution_by_Linde_F_K_zeolite_prepared_from_recycled_fly_ash

Chen, C., Cheng, T., Zhang, X., Wu, R. & Wang, Q. (2019a). Synthesis of an Efficient Pb Adsorption Nano-Crystal under Strong Alkali Hydrothermal Environment Using a Gemini Surfactant as Directing Agent. *Journal of the Chemical Society of Pakistan*, 41,6, pp. 1034–1038.

Chen, C., Chenhao, Y., Ting, C., Xiao, Z. & Jiandong, Z. (2019b). Preparation of Mo-Na composite catalyst and its application in pharmaceutical wastewater treatment. *Industrial Water Treatment*, 39, 8, pp. 77–81. (in Chinese)

Chen, C., Jiandong, Z., Ting, C. & Xiao, Z. (2018). Preparation of Nano-manganese Cerium/γ-Al2O3 Composite Catalyst and Its Catalytic Wet Air Oxidation Treatment of Antibiotic Production Wastewater. *Journal of Synthetic Crystals*, 47,11, pp. 2288–2294. (in Chinese)

Chen, C., Li, Q., Shen, L. & Zhai, J. (2012). Feasibility of manufacturing geopolymer bricks using circulating fluidized bed combustion bottom ash. *Environ Technol*, 33, 10–12, pp. 1313–1321. DOI: 10.1080/09593330.2011.626797

Chen, M., Ren, L., Qi, K., Li, Q., Lai, M., Li, Y., Li, X. & Wang, Z. (2020). Enhanced removal of pharmaceuticals and personal care products from real municipal wastewater using an electrochemical membrane bioreactor. *Bioresource Technology*, 311,123579. DOI: 10.1016/j.biortech.2020.123579

Cheng, T., Chen, C., Tang, R., Han, C.-H. & Tian, Y. (2018). Competitive Adsorption of Cu, Ni, Pb, and Cd from Aqueous Solution Onto Fly Ash-Based Linde F(K) Zeolite. *Iranian Journal of Chemistry & Chemical Engineering – International English Edition*, 37,1, pp. 61–72. DOI: 10.30492/IJCCE.2018.31971

Cheng, T., Chen, C., Wang, L., Zhang, X., Ye, C., Deng, Q. & Chen, G. (2021). Synthesis of Fly Ash Magnetic Glass Microsphere@BiVO4 and Its Hybrid Action of Visible-Light Photocatalysis and Adsorption Process. *Polish Journal of Environmental Studies*, 30, 3, pp. 1–14. DOI: 10.15244/pjoes/127918

Coimbra, R.N., Calisto, V., Ferreira, C.I.A., Esteves, V.I. & Otero, M. (2019). Removal of pharmaceuticals from municipal wastewater by adsorption onto pyrolyzed pulp mill sludge. *Arabian Journal of Chemistry*, 12, 8, pp. 3611–3620. DOI: 10.1016/j.arabjc.2015.12.001

Dong, S., Cui, L., Zhang, W., Xia, L. & Sun, J.J.C.E.J. (2020). Double-shelled ZnSnO3 hollow cubes for efficient photocatalytic degradation of antibiotic wastewater. *Chemical engineering journal*, 384,123279. DOI: 10.1016/j.cej.2019.123279

Ferrer-Polonio, E., Fernandez-Navarro, J., Iborra-Clar, M.-I., Alcaina-Miranda, M.-I. & Antonio Mendoza-Roca, J. (2020). Removal of pharmaceutical compounds commonly-found in wastewater through a hybrid biological and adsorption process. *Journal of Environmental Management*, 33, 3, pp. 29–35. DOI: 10.1016/j.jenvman.2020.110368

Guo, J., Fortunato, L., Deka, B.J., Jeong, S. & An, A.K. (2020). Elucidating the fouling mechanism in pharmaceutical wastewater treatment by membrane distillation. *Desalination*, 475,114148. DOI: 10.1016/j.desal.2019.114148

He, Y., Chen, Y.-G., Zhang, K.-N., Ye, W.-M. & Wu, D.-Y. (2019). Removal of chromium and strontium from aqueous solutions by adsorption on laterite. *Archives of Environmental Protection*, 45, 3, pp. 11–20. DOI 10.24425/aep.2019.128636

Hofman-Caris, C.H.M., Siegers, W.G., van de Merlen, K., de Man, A.W.A. & Hofman, J.A.M.H. (2017). Removal of pharmaceuticals from WWTP effluent: Removal of EfOM followed by advanced oxidation. *Chemical Engineering Journal*, 327, 1, pp. 514–521. DOI: 10.1016/j.cej.2017.06.154

Hohenberg, P. & Kohn, W. (1964). InhomogeIIeous Electron Gas. *Physical Review*, 136, 3B, pp. 864–871.

Huang, J., Wang, X., Li, S. & Wang, Y. (2010). ZnO/MoO3 mixed oxide nanotube: A highly efficient and stable catalyst for degradation of dye by air under room conditions. Applied Surface Science, 257,1, pp. 116–121. DOI: 10.1016/j.apsusc.2010.06.046

Huang, P.R., He, Y., Cao, C. & Lu, Z.H. (2014). Impact of lattice distortion and electron doping on alpha-MoO3 electronic structure. *Sci Rep.*, 4,7131, pp. 1–7. DOI: 10.1038/srep07131

Kang, J., Zhan, W., Li, D., Wang, X., Song, J. & Liu, D. (2011). Integrated catalytic wet air oxidation and biological treatment of wastewater from Vitamin B-6 production. *Physics and

Chemistry of the Earth, 36, 9–11, pp. 455–458. DOI: 10.1016/j. pce.2010.03.043

Khan, A.H., Khan, N.A., Ahmed, S., Dhingra, A., Singh, C.P., Khan, S.U., Mohammadi, A.A., Changani, F., Yousefi, M., Alam, S., Vambol, S., Vambol, V., Khursheed, A. & Ali, I. (2020). Application of advanced oxidation processes followed by different treatment technologies for hospital wastewater treatment. *Journal of Cleaner Production*, 269,122411. DOI: 10.1016/j.jclepro.2020.122411

Klancar, A., Trontelj, J., Kristl, A., Meglic, A., Rozina, T., Justin, M.Z. & Roskar, R. (2016). An advanced oxidation process for wastewater treatment to reduce the ecological burden from pharmacotherapy and the agricultural use of pesticides. *Ecological Engineering*, 97, 186–195. DOI: 10.1016/j.ecoleng.2016.09.010

Kohn, W. & Sham, L.J. (1965). Self-Consistent Equations Including Exchange and Correlation Effects. *Physical Review*, 140, A1133.

Kresse, G. & Furthmuller, J. (1996). Efficient iterative schemes for ab initio total-energy calculations using a plane-wave basis set. *Physical review. B, Condensed matter*, 54, 16, pp. 11169–11186.

Li, W., Zhao, S., Qi, B., Du, Y., Wang, X. & Huo, M. (2009). Fast catalytic degradation of organic dye with air and MoO3:Ce nanofibers under room condition. *Applied Catalysis B-Environmental*, 92, 3–4, pp. 333–340. DOI: 10.1016/j.apcatb.2009.08.012

Li, Y., Shen, J., Quan, W., Diao, Y., Wu, M., Zhang, B., Wang, Y. & Yang, D. (2020). 2D/2D p-n Heterojunctions of CaSb2O6/g-C(3) N(4)for Visible Light-Driven Photocatalytic Degradation of Tetracycline. *European Journal of Inorganic Chemistry*, 2020, 40, pp. 3852–3858. DOI: 10.1002/ejic.202000635

Tan, l., Yu, C., Wang, M., Zhang, S. & Sun, J., Dang, S. & Sun, J. (2019). Synergistic effect of adsorption and photocatalysis of 3D g-C3N4-agar hybrid aerogels. *Applaied Surface Science*, 467–468, pp. 286–292. DOI: 10.1016/j.apsusc.2018.10.067

Lunagomez Rocha, M.A., Del Angel, G., Torres-Torres, G., Cervantes, A., Vazquez, A., Arrieta, A. & Beltramini, J.N. (2015). Effect of the Pt oxidation state and Ce3+/Ce4+ ratio on the Pt/TiO2-CeO2 catalysts in the phenol degradation by catalytic wet air oxidation (CWAO). *Catalysis Today*, 250, 145–154. DOI: 10.1016/j.cattod.2014.09.016

Ma, Y., Jia, Y., Jiao, Z., Wang, L., Yang, M., Bi, Y. & Qi, Y. (2015). Facile synthesize α-MoO3 nanobelts with high adsorption property. *Materials Letters*, 157, 53–56. DPOI: 10.1016/j.matlet.2015.05.095

Mucha, Z. & Kułakowski, P. (2016). Turbidity measurements as a tool of monitoring and control of the SBR effluent at the small wastewater treatment plant – preliminary study. *Archives of Environmental Protection*, 42,3, pp. 33–36. DOI 10.1515/aep-2016-0030

Mukimin, A., Vistanty, H. & Zen, N. (2020). Hybrid advanced oxidation process (HAOP) as highly efficient and powerful treatment for complete demineralization of antibiotics. *Separation and Purification Technology*, 241, 116728. DOI: 10.1016/j.seppur.2020.116728

Parvas, M., Haghighi, M. & Allahyari, S. (2019). Catalytic wet air oxidation of phenol over ultrasound-assisted synthesized Ni/CeO2-ZrO2 nanocatalyst used in wastewater treatment. *Arabian Journal of Chemistry*, 12, 7, pp. 1298–1307. DOI: 10.1016/j.arabjc.2014.10.043

Perdew, J., Burke, K. & Ernzerhof, M. (1996). Generalized Gradient Approximation Made Simple. *Physical review letters*, 77, 3865–3868. DOI: 10.1103/PhysRevLett.77.3865

Perdew, J.P., Chevary, J.A., Jackson, K.A., Pederson, M.R., Singh, D.J. & Fiolhais, C. (1992). Atoms, Molecules, Solids, and Surfaces: Applications of the Generalized Gradient Approximation for

Exchange and Correlation. *Physical review. B, Condensed matter*, 46, 6671–6687.

Phoon, B.L., Ong, C.C., Saheed, M.S.M., Show, P.-L., Chang, J.-S., Ling, T. C., Lam, S.S. & Juan, J.C. (2020). Conventional and emerging technologies for removal of antibiotics from wastewater. *Journal of Hazardous Materials*, 400, 122961. DOI: 10.1016/j.jhazmat.2020.122961

Schrank, S.G., Jose, H.J., Moreira, R.F.P.M. & Schroder, H.F. (2004). Elucidation of the behavior of tannery wastewater under advanced oxidation conditions. *Chemosphere*, 56, 5, pp. 411–23. DOI: 10.1016/j.chemosphere.2004.04.012

Sushma, Kumari, M. & Saroha, A.K. (2018). Treatment of toxic industrial effluent containing nitrogenous organic compounds by integration of catalytic wet air oxidation at atmospheric pressure and biological processes. *Journal of Environmental Chemical Engineering*, 6, 5, pp. 6256–6262. DOI: 10.1016/j.jece.2018.09.057

Urbanowska, A. & Kabsch-Korbutowicz, M. (2019). Nanofiltration as an effective method of NaOH recovery from regenerative solutions. *Archives of Environmental Protection*, 45,2, pp. 31–36. DOI: 10.24425/aep.2019.127978

Verma, A., Kaur, H. & Dixit, D. (2013). Photocatalytic, Sonolytic and Sonophotocatalytic Degradation of 4-Chloro-2-Nitro Phenol. *Archives of Environmental Protection*, 39,2, pp. 17–28. DOI: 10.2478/aep-2013-0015

Wang, G., Wang, D., Xu, Y., Li, Z. & Huang, L. (2020a). Study on optimization and performance of biological enhanced activated sludge process for pharmaceutical wastewater treatment. *Science of the Total Environment*, 739,140166. DOI: 10.1016/j.scitotenv.2020.140166

Wang, J., Dong, S., Yu, C., Han, X., Guo, J. & Sun, J. (2017). An efficient MoO3 catalyst for in-practical degradation of dye wastewater under room conditions. *Catalysis Communications*, 92, 100–104. DOI: 10.1016/j.catcom.2017.01.013

Wang, P., Liang, Y.N., Zhong, Z. & Hu, X. (2020b). Nano-hybrid bimetallic Au-Pd catalysts for ambient condition-catalytic wet air oxidation (AC-CWAO) of organic dyes. *Separation and Purification Technology*, 233, 15, pp. 11590. DOI: 10.1016/j.seppur.2019.115960

Xu, K., Liao, N., Zheng, B. & Zhou, H. (2020). Adsorption and diffusion behaviors of H2, H2S, NH3, CO and H2O gases molecules on MoO3 monolayer: A DFT study. *Physics Letters A*, 384,21, pp. 1–5. DOI: 10.1016/j.physleta.2020.126533

Yadav, A., Teja, A.K. & Verma, N. (2016). Removal of phenol from water by catalytic wet air oxidation using carbon bead – supported iron nanoparticle – containing carbon nanofibers in an especially configured reactor. *Journal of Environmental Chemical Engineering*, 4, 2, pp. 1504–1513. DOI: 10.1016/j.jece.2016.02.021

Zhang, X., Cheng, T., Chen, C., Wang, L., Deng, Q., Chen, G. & Ye, C. (2020). Synthesis of a novel magnetic nano-zeolite and its application as an efficient heavy metal adsorbent. *Materials Research Express*, 7, 8, pp. 085007. DOI: 10.1088/2053-1591/abab43

Zhang, Y., Zhang, Z., Yan, Q. & Wang, Q. (2016). Synthesis, characterization, and catalytic activity of alkali metal molybdate/α-MoO3 hybrids as highly efficient catalytic wet air oxidation catalysts. *Applied Catalysis A: General*, 511, 47–58. DOI: 10.1016/j.apcata.2015.11.035

Zou, H., Ma, W. & Wang, Y. (2015). A novel process of dye wastewater treatment by linking advanced chemical oxidation with biological oxidation. *Archives of Environmental Protection*, 41, 4, pp. 33–39. DOI: 10.1515/aep-2015-0037